Volume 5
Number 5
May 2026
Pages 615–750

Sensors & Diagnostics

rsc.li/sensors

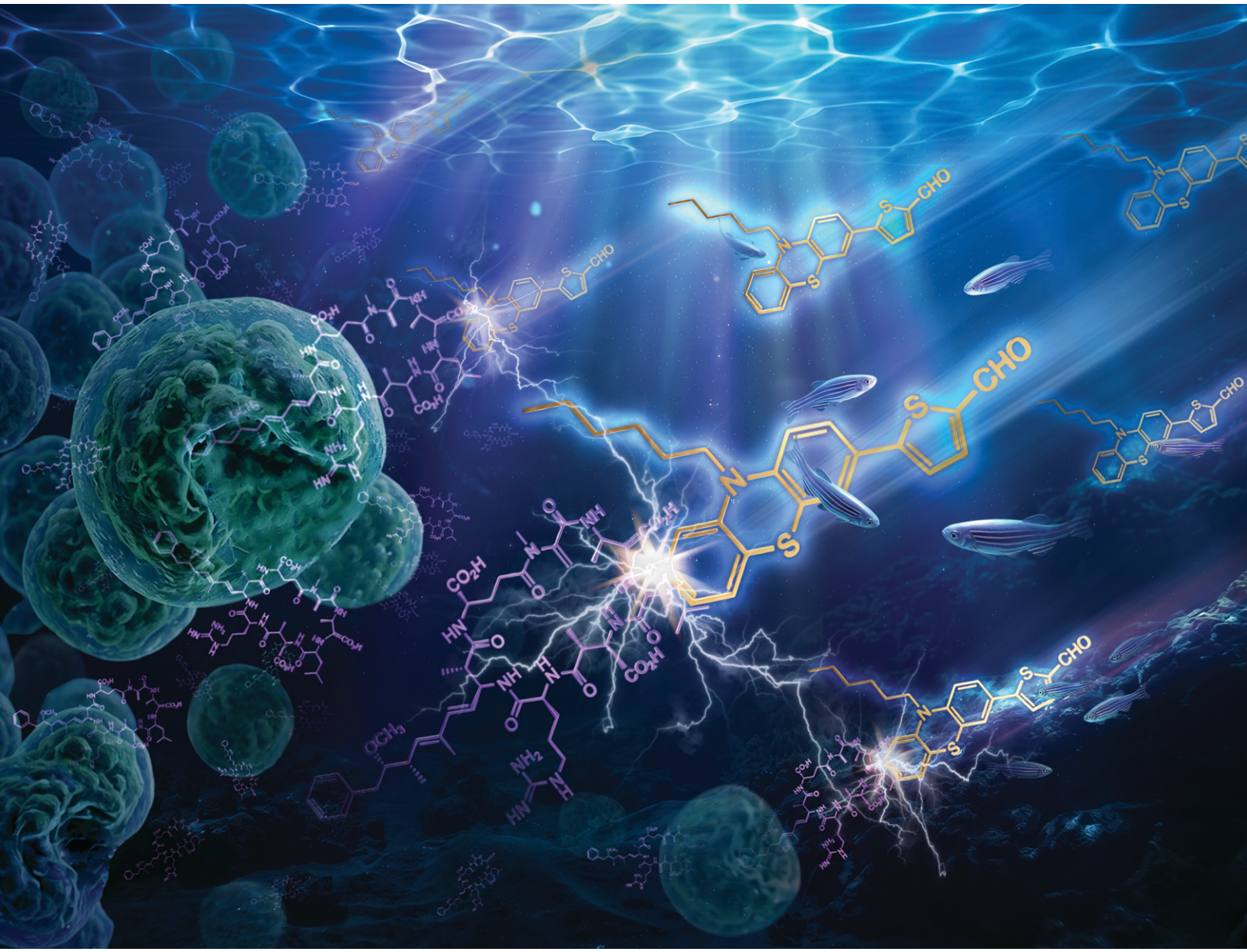

ISSN 2635-0998

ROYAL SOCIETY OF CHEMISTRY

PAPER

Xiao Yao and Zhuwu Jiang *et al.*
Design and mechanistic study of a high-sensitivity small-molecule fluorescent probe for the detection of microcystin-LR

Sensors & Diagnostics

PAPER

View Article Online
View Journal | View Issue

Cite this: *Sens. Diagn.*, 2026, **5**, 687

Design and mechanistic study of a high-sensitivity small-molecule fluorescent probe for the detection of microcystin-LR

Jinfeng Chen,†[a] Zhicen Qiu,†[a] Linyu Fan,†[bc] Yisang Lu,[a] Silong Li,[a] Yuxin Yang,[a] Wanhe Wang,[f] Cheuk-Lam Ho,*[bc] Xiao Yao*[ade] and Zhuwu Jiang*[a]

Cyanobacterial bloom-derived microcystin-LR (MC-LR) poses serious threats to aquatic ecosystems and human health, while conventional analytical methods often require expensive instrumentation and labor-intensive procedures. Herein, we report a small-molecule fluorescent probe for MC-LR detection, synthesized *via* a simplified route and structurally confirmed by ^{1}H NMR, ^{13}C NMR, FT-IR and HRMS. The probe exhibited a concentration-dependent fluorescence enhancement toward MC-LR over 0–100 μM with good linearity (R^2 = 0.982) and a low detection limit of 0.507 μM. Reliable performance was maintained under near-neutral conditions (pH 6–9), along with excellent photostability and strong anti-interference capability against 10 common amino acids. Zebrafish embryo assays further demonstrated low toxicity of the probe. Mechanistic investigations suggest that the fluorescence response arises from synergistic recognition driven by π–π stacking interactions between the probe and the aromatic moieties of MC-LR, together with long-chain binding dominated by hydrophobic association with the aliphatic segment of MC-LR, which facilitates electron transfer and amplifies the emission signal. Overall, this probe provides a rapid and reliable platform for MC-LR detection in practical water matrices.

Received 12th February 2026,
Accepted 19th April 2026

DOI: 10.1039/d6sd00036c

rsc.li/sensors

1. Introduction

Eutrophication-driven cyanobacterial blooms have become a major environmental issue threatening freshwater ecosystems and drinking-water safety, largely because many bloom-forming cyanobacteria can produce microcystins (MCs). MCs are hepatotoxic cyclic peptide toxins, and more than 200 variants have been reported.[1–5] Among them, microcystin-LR (MC-LR) is recognized as one of the most toxic and widely distributed cyanobacterial toxins. MC-LR can enter the human body *via* the gastrointestinal tract and has been associated with symptoms such as diarrhea, neurological dysfunction, and liver injury.[6–8] At high exposure levels in aquatic systems, it also poses serious risks to aquatic organisms and may lead to poisoning or mortality events.[9,10] Structurally, MC-LR is a cyclic heptapeptide composed of seven amino-acid residues; this architecture contributes to its high chemical stability and persistence in aquatic environments.[11,12] To reduce human exposure risks, both the Chinese drinking-water standard (GB 5749-2006) and the World Health Organization set the maximum allowable concentration of microcystins in drinking water at 1 μg L^{-1}, underscoring the necessity of reliable MC-LR monitoring in aquatic matrices.[13,14]

At present, conventional analytical methods for MC-LR determination mainly include high-performance liquid chromatography (HPLC), liquid chromatography–mass spectrometry (LC–MS), protein phosphatase inhibition assay (PPIA), and enzyme-linked immunosorbent assay (ELISA).[11,15–18] Although these methods generally provide good accuracy, they often suffer from limitations such as time-consuming procedures, strong dependence on sophisticated instrumentation, and high operational costs, which restrict their use in rapid on-site detection and high-throughput screening.[19–21] Therefore, to address industrial and laboratory needs, it is imperative to develop molecular recognition strategies that integrate structural complementarity with strong interactions while enabling efficient signal transduction.[22–25] In recent years, fluorescent

[a] *School of Ecological Environment and Urban Construction, Fujian University of Technology, Fuzhou, Fujian, PR China. E-mail: yaoxiao0520@gmail.con, jiangzhuwu@fjut.edu*
[b] *Department of Applied Biology and Chemical Technology, The Hong Kong Polytechnic University, Hung Hom, Hong Kong, China. E-mail: cheuk-lam.ho@polyu.edu.hk*
[c] *PolyU Shenzhen Research Institute, Shenzhen, China*
[d] *Fujian Key Laboratory of Leather Green Design and Manufacture, Jinjiang 362271, China*
[e] *National Enterprise Technical Center, Xingye Leather Technology Co. Ltd., Jinjiang 362261, China*
[f] *School of Life Science and Techonology, Northwestern Polytechnical University, 127 West Youyi Road, Xi'an, Shannxi 710072, China*
† These authors contributed equally to this work.

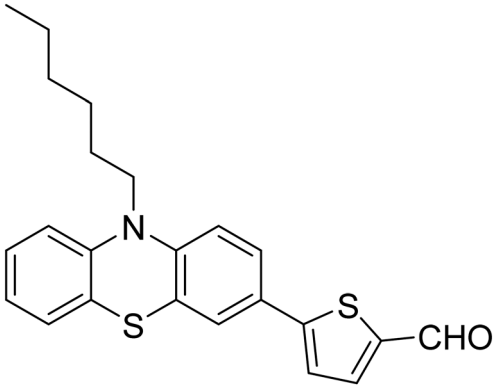

Fig. 1 Schematic diagram of the probe structure.

probes have attracted increasing attention for environmental analysis because molecular recognition can be converted into visible and quantifiable optical outputs.[26–29] However, the development of small-molecule fluorescent probes for MC-LR remains challenging: the large cyclic scaffold and multiple potential interaction sites complicate the construction of effective recognition motifs; moreover, because MC-LR is composed of amino-acid residues, free amino acids and related biomolecules in complex samples may cause interference and compromise selectivity.[24,30–34]

To overcome these challenges, we report a small-molecule fluorescent probe (Fig. 1) that specifically recognizes MC-LR *via* cooperative π–π stacking interactions and long-chain binding between the probe and MC-LR. Titration experiments show that the fluorescence intensity of the probe increases progressively with increasing MC-LR concentration, and the fluorescence response exhibits a good linear relationship with MC-LR concentration and the maximum fluorescence intensity. In addition, the probe maintains stable fluorescence in phosphate-buffered saline (PBS) over a pH range of 6–9. Anti-interference experiments further demonstrate high specificity toward MC-LR in the presence of various amino acids, indicating adequate stability and interference tolerance for complex matrices and natural waters.[35] XPS was also employed to elucidate and corroborate the detection mechanism. Finally, zebrafish embryo toxicity assays confirm its environmental safety for applications in natural-water settings. Collectively, this probe provides a convenient and rapid tool for qualitative and quantitative analysis of MC-LR in environmental samples and offers additional insight into MC-LR recognition mechanisms, with promising potential for practical water-body monitoring.

2. Materials and methods

2.1. Synthesis of the probe

The probe was synthesized by the Suzuki reaction of (10-hexanoyl-10H-phenothiazin-3-yl)boronic acid and 5-bromothiophene-2-carbaldehyde; the synthesis route of the probe is illustrated in Scheme 1. Characterization techniques (*i.e.* ^{1}H NMR, ^{13}C NMR, HRMS, and FTIR) are detailed in the SI, alongside the respective data (*i.e.* Fig. S1–S4 and Table S1).

2.2. MC-LR concentration titration experiment

MC-LR standard solutions (stock concentration: 500 μM; 0, 5, 10, 15, 20, 25, 30, 35, and 40 μL) were sequentially added into PCR tubes and diluted with purified water to a final volume of 200 μL. Based on the stock concentration and the added volume, the final concentrations of the prepared MC-LR solutions were calculated to range from 0 to 100 μM. The probe was dissolved in DMSO to prepare a 10 mM stock solution. Subsequently, 2 μL of the probe stock solution was added to each sample, and the mixtures were thoroughly vortexed. The fluorescence intensity and UV-vis absorption spectra of the samples were then recorded using a fluorescence spectrophotometer and a UV-vis spectrophotometer, respectively. Finally, a response curve was constructed by plotting the fluorescence intensity at the maximum emission wavelength (607 nm) against the corresponding MC-LR concentration, and the concentration-dependent response was analyzed.

2.3. Probe stability detection experiment

Given that the pH of natural water bodies typically ranges from 6 to 9,[36] phosphate-buffered saline (PBS) solutions with pH values of 6.0, 6.5, 7.0, 7.5, 8.0, 8.5, and 9.0 were prepared to evaluate the spectral response of the probe across this pH range. Fluorescence emission spectra were collected at the maximum excitation wavelength (350 nm), and the corresponding maximum emission wavelengths at each pH were extracted and summarized in bar charts to analyze their variation trends. In parallel, the probe solution was continuously irradiated at the maximum excitation wavelength for 30 min; changes in the maximum emission wavelength were monitored and the emission spectra were recorded to assess the photostability of the probe.

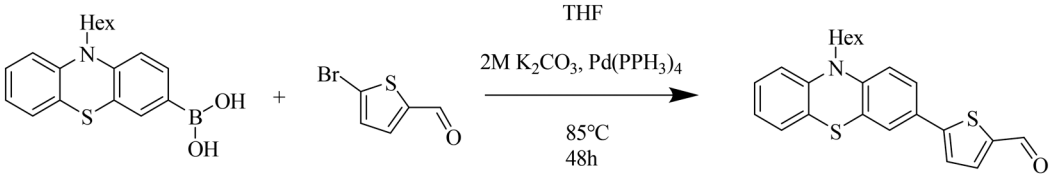

Scheme 1 The synthesis route for probe fabrication.

2.4. Probe anti-interference detection experiment

Since MC-LR is a cyclic heptapeptide containing seven amino acids,[37] amino acids were selected as the primary organic interferents in the anti-interference experiment of the probe. Meanwhile, to further evaluate the selectivity and anti-interference performance of the probe in complex environmental systems, common metal ions and humic acid were also introduced as additional interferents. Among them, the standard solutions of 10 common amino acids (Cys, Pro, Glu, Arg, Thr, Ser, Asp, Asn, Ile, and His) and humic acid were prepared at concentrations of 500 μM, while the standard solutions of common metal ions were prepared at 100 μg mL^{-1}. The selected metal ions included Mg^{2+}, Ca^{2+}, Fe^{3+}, Al^{3+}, As^{3+}, Ba^{2+}, Cd^{2+}, Li^{+}, and Zn^{2+}. In the experiment, 50 μL of each interferent standard solution was separately added into PCR tubes, followed by the addition of purified water to a final volume of 200 μL. Subsequently, 2 μL of the probe standard solution was added to each PCR tube. After thorough mixing by shaking, the changes in fluorescence intensity and UV-vis absorption spectra were recorded using a fluorescence spectrophotometer and a UV-vis spectrophotometer, respectively, in order to evaluate the interference effects of different coexisting substances on the probe-based detection of MC-LR.

2.5. Toxicity testing experiments

All animal procedures were performed in accordance with the Guidelines for Care and Use of Laboratory Animals of Fujian University of Technology and approved by the Animal Ethics Committee of Fujian University of Technology. Zebrafish embryos were used to preliminarily evaluate the biocompatibility of the probe. Ten embryos were placed in each well of a multiwell plate, followed by the addition of 100 μL of probe solution and 900 μL of zebrafish embryo hatching medium (total volume: 1000 μL per well). The control group contained embryos incubated in hatching medium only (1000 μL per well). Each condition was tested in triplicate. Embryo twitching frequency at 24 h, heart rate at 48 h, and survival rate at 72 h were recorded under a microscope. The results were compared with the control group and presented as bar charts.

3. Results and discussion

3.1. Probe response to MC-LR concentration changes

To validate the probe's suitability for detecting MC-LR in solution, we measured its absorption spectrum in aqueous solutions with varying MC-LR concentrations. The probe exhibited a primary absorption peak within the 500–690 nm range, with its maximum emission peak exhibiting a red shift as the MC-LR concentration increased. Experimental results demonstrated that the fluorescence intensity of the probe solution progressively increased with increasing MC-LR concentration in the solution. Plotting the maximum emission wavelength of the probe solution against the MC-LR concentration and performing linear fitting revealed a good linear correlation between the maximum emission wavelength and MC-LR concentration. Calculations indicated that the detection limit of this probe is 0.507 μM, demonstrating its high sensitivity toward MC-LR in aqueous solutions. Therefore, the probe possesses sufficient sensitivity to enable simple and rapid qualitative and quantitative detection of MC-LR (Fig. 2).

3.2. Probe stability and anti-interference testing

To examine the probe performance under environmentally relevant conditions, we first investigated its pH tolerance. Considering that the pH of most natural waters generally falls within 6–9,[36] PBS buffers with pH values of 6.0, 6.5, 7.0, 7.5, 8.0, 8.5, and 9.0 were used to evaluate the pH-dependent optical response of the probe. As shown in Fig. 3a, under

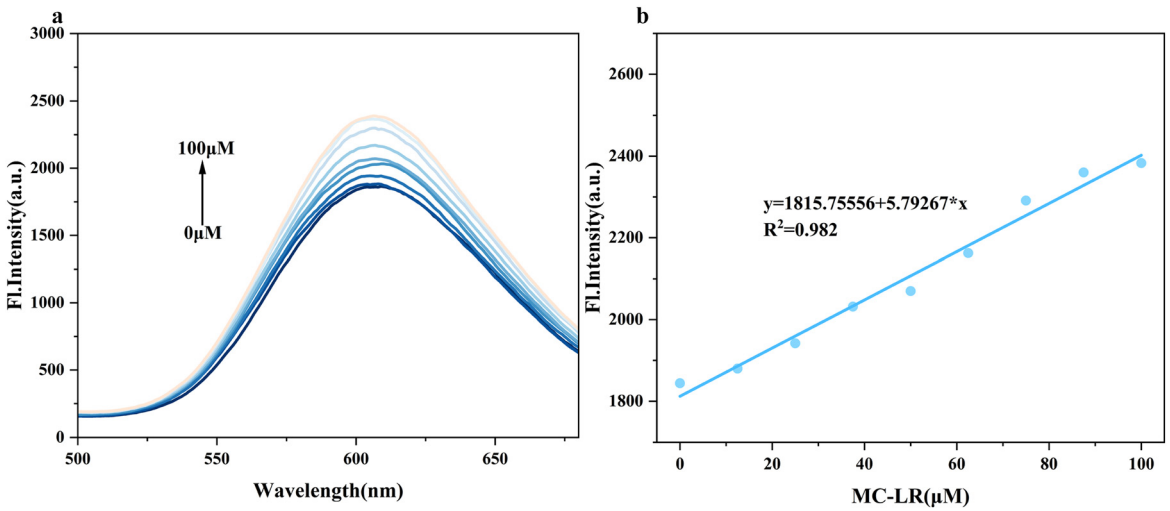

Fig. 2 (a) Emission spectra of the probe in solutions with different concentrations of MC-LR; (b) linear relationship between the maximum emission wavelength and the concentration of MC-LR.

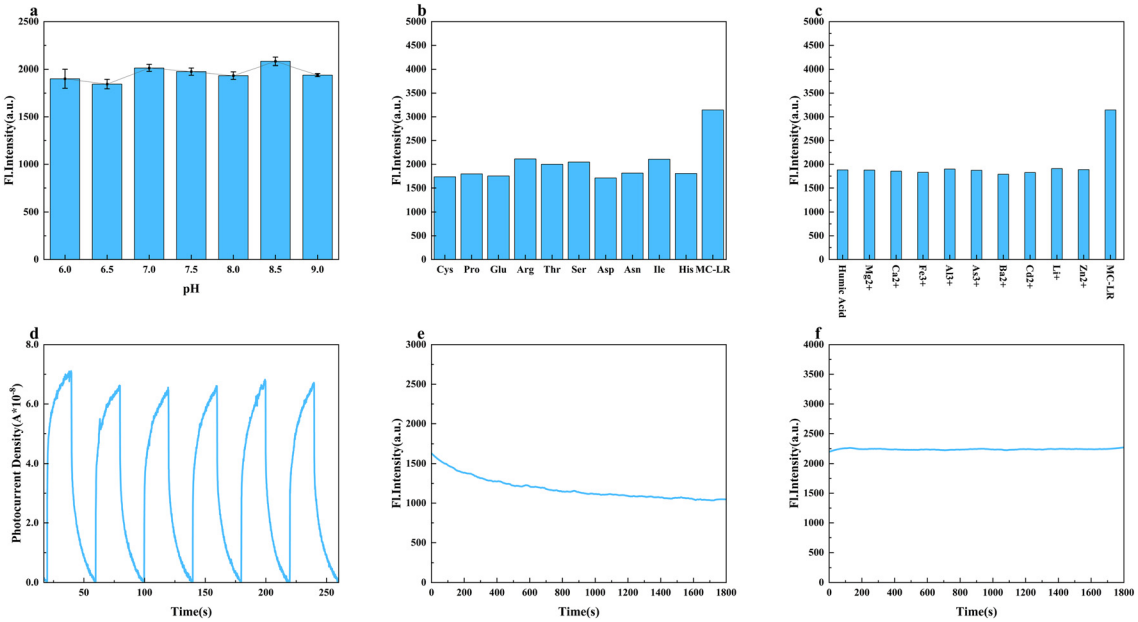

Fig. 3 (a) Histogram of the fluorescence intensity at the maximum emission wavelength of the probe after the addition of the probe standard solution in PBS buffer solutions with different pH values; (b) histogram of the fluorescence intensity at the maximum emission wavelength of the probe in solutions containing different amino acids; (c) histogram of the fluorescence intensity at the maximum emission wavelength of the probe in solutions containing humic acid as well as anions and cations; (d) photocurrent density curve of the probe; (e) variation in the fluorescence intensity at the emission wavelength of the probe under continuous irradiation for 30 min at a fixed excitation wavelength; (f) variation in the fluorescence intensity at the emission wavelength of the probe–MC-LR mixed solution under continuous irradiation for 30 min at a fixed excitation wavelength.

excitation at 350 nm, the probe exhibited an identical emission maximum at 607 nm throughout the tested pH range, and the fluorescence intensity remained essentially unchanged, indicating negligible pH interference and good signal stability in typical natural-water environments.

Subsequently, the selectivity of the probe was evaluated in the presence of potential coexisting interferents. Given that MC-LR is a cyclic heptapeptide composed of seven amino acid residues, representative amino acids were selected as the primary interferents for the anti-interference study. Meanwhile, to better simulate complex natural-water environments, humic acid as well as common metal ions were also introduced as additional interferents. As shown in Fig. 3b, the probe generated only weak fluorescence responses in the presence of various amino acids. In addition, as shown in Fig. 3c, the probe likewise exhibited only weak fluorescence signals in the presence of humic acid and common anions and cations, whereas a markedly enhanced fluorescence response was observed in the presence of MC-LR. These results demonstrate the high selectivity of the probe toward MC-LR and its good anti-interference capability.

The photostability of the probe was further evaluated under continuous irradiation at 350 nm. As shown in Fig. 3e, no obvious attenuation in the fluorescence intensity was observed after continuous irradiation for 30 min, indicating that the probe possesses excellent resistance to photobleaching. In addition, as shown in Fig. 3f, the fluorescence intensity of the probe–MC-LR mixed solution also showed no significant decrease after continuous irradiation for 30 min at a fixed excitation wavelength, indicating good stability of the system after interaction with MC-LR. Meanwhile, the photocurrent measurements (Fig. 3d) displayed stable responses under illumination, further confirming the robustness of the probe.

Finally, a simple proof-of-concept demonstration was performed by writing patterns on blank paper using aqueous solutions (Fig. S12). The clear and stable patterns obtained indicate the feasibility of the probe for practical operation, supporting its potential for real-world and application-oriented sensing.

3.3. Toxicity testing experiments

In this experiment, we used zebrafish embryos as a model to assess the biological toxicity of the probe in terms of the survival rate, movement frequency, and heart rate.[38] The results showed that the survival rates in both the control and probe groups remained high, with no significant differences. Similarly, no significant changes were observed in the twitching frequency or heart rate. This indicates that under the experimental exposure conditions, the probe exhibited no acute lethal toxicity or teratogenic effects, and it did not cause significant damage to zebrafish survival capacity or developmental morphology. Additionally, the probe did not interfere with zebrafish's basic motor abilities, and their

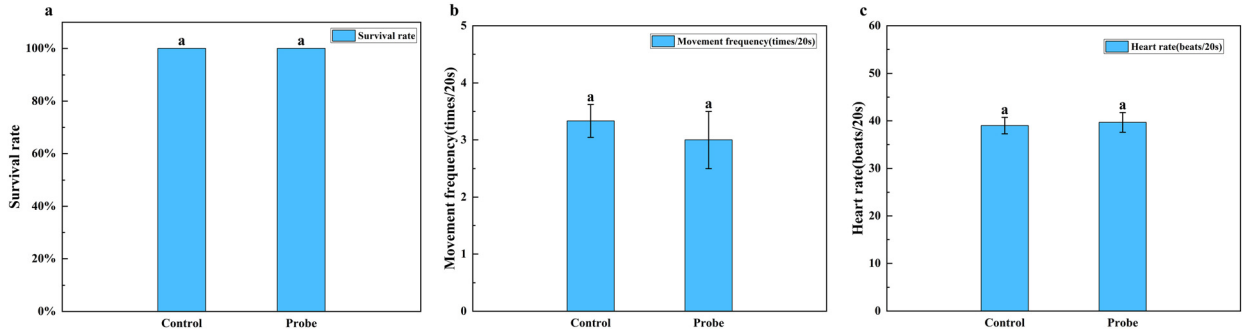

Fig. 4 (a) Survival rate, (b) movement frequency and (c) heart rate of zebrafish eggs under the conditions of the blank group and probe group.

muscular system remained largely unaffected.[39] These findings suggest that the probe has low toxicity and good environmental compatibility, making it a viable candidate for monitoring natural water bodies (Fig. 4).

3.4. Luminescence mechanism

This probe was designed as a small-molecule fluorescence sensor for targeted recognition of microcystin-LR (MC-LR) by integrating multiple noncovalent interactions (C–H···π, NH···π, and C–H···O) along with a long-chain binding effect. Considering that MC-LR is a cyclic heptapeptide composed of seven amino-acid residues, it contains multiple amide bonds and adjacent C–H groups. The electronegativity of the amide bond can polarize the neighboring C–H bonds, thereby enhancing the CH–O interactions between these polarized C–H groups and the carbazole moiety of the probe. Meanwhile, the N–H and C–H groups in the amino-acid residues of MC-LR may also interact with the benzene rings of the probe through NH–π and CH–π interactions. Based on these considerations, the fluorescence enhancement may be attributed to the following synergistic effects: (i) the binding/association of C–H and N–H groups from MC-LR with the aromatic rings of the probe, (ii) CH–O interactions between the C–H groups of the probe and the amide carbonyl oxygen atoms of MC-LR, and (iii) the synergistic stabilization effect resulting from the binding of the probe's long-chain segment to the cyclic scaffold of MC-LR.

According to the DFT calculations (Fig. 5 and 6), the HOMO–LUMO energy levels of the probe and the probe–MC-LR complex were evaluated to elucidate the sensing mechanism. The results showed that the HOMO energy level shifted from −5.24 eV (free probe) to −5.21 eV upon interaction with MC-LR. This energetic alignment, combined with the electron density rearrangement revealed by XPS, suggests that the synergistic non-covalent interactions—including C–H···O, C–H···π, and N–H···π stacking as well as the long-chain binding—effectively stabilized the excited state. These interactions significantly restrict the intramolecular rotation of the probe, thereby suppressing nonradiative relaxation pathways and

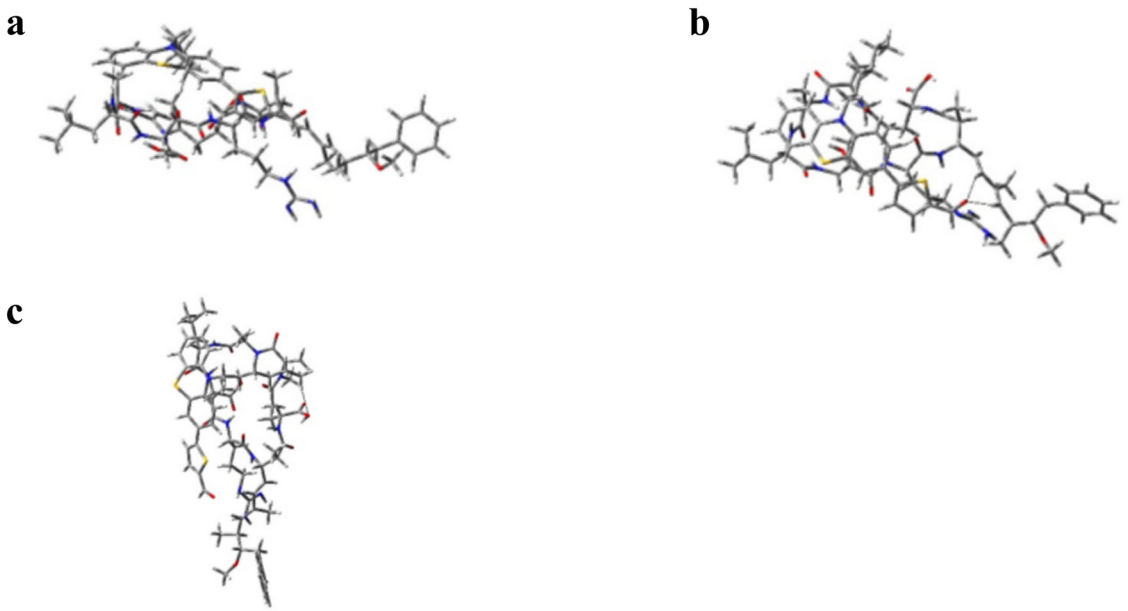

Fig. 5 (a) Diagram of the N–H···π and C–H···π interactions formed between MC-LR and the probe; (b) diagram of the C–H···O interaction formed between MC-LR and the probe; (c) diagram of the C–H···O interaction formed between the long chain and MC-LR.

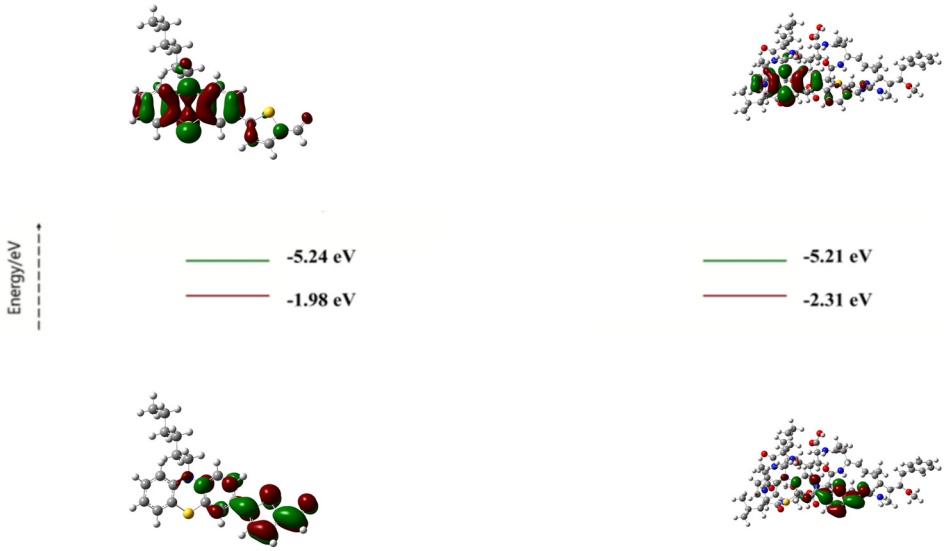

Fig. 6 Electron cloud diagrams of the probe before and after reaction with MC-LR.

prolonging the excited-state lifetime. Consequently, the radiative transition probability is enhanced, leading to the observed fluorescence amplification. In addition, significant C–H···O, C–H···π, and N–H···π interactions, as well as interactions between the long chain and MC-LR, were observed between the probe molecule and the MC-LR molecule.

XPS analysis was conducted to study the interaction between the probe and microcystin-LR (Fig. 7), revealing significant changes in the binding energies and peak shapes of the C, N, O, and S elements, indicating electronic density rearrangement and changes in the chemical environment. In the C 1s spectrum, before interaction with the toxin, the main peak at 284.80 eV was attributed to C–C/C=C bonds in the carbazole and thiophene groups, while the characteristic peak at 285.88 eV corresponded to the C–S bond in the thiophene unit, and the weak peak at 288.48 eV was attributed to the C=O bond. After binding with MC-LR, a new C–O characteristic peak appeared at 287.93 eV, and the binding energy increased, indicating a decrease in the electron density of some carbon atoms, which is associated with electron transfer between the probe's aromatic ring and the polarized C–H groups of the MC-LR amide bond, leading to the formation of C–H···O interactions.[40] In the N 1s spectrum, before interaction, the single peak at 399.83 eV corresponded to the pyrrole-type nitrogen in the carbazole

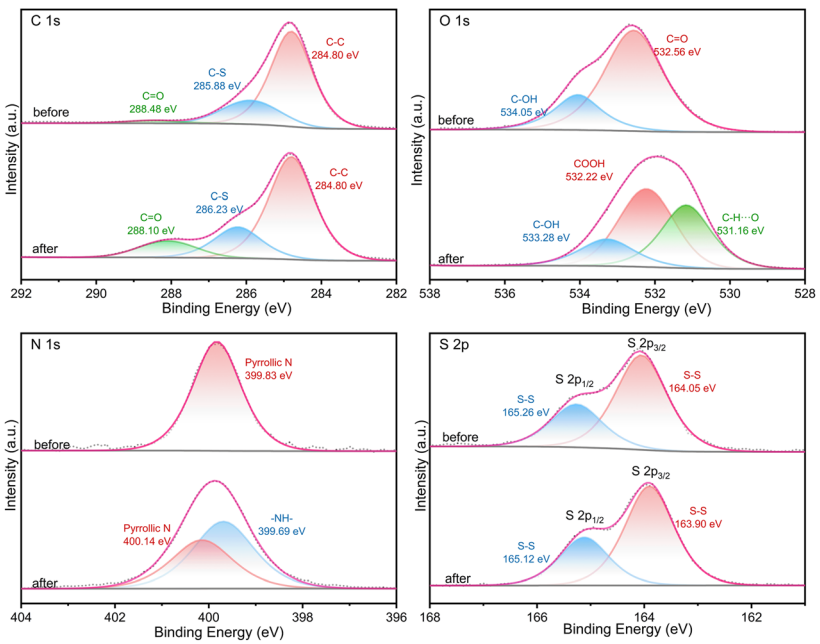

Fig. 7 XPS spectra of the probe before and after the reaction.

moiety. After exposure to the toxin, this peak shifted to a higher binding energy at 400.14 eV, while a new peak appeared at 399.69 eV, indicating two nitrogen environments. The peak at 400.14 eV, corresponding to the pyrrole nitrogen, showed a higher binding energy, suggesting a decrease in the electron density of the nitrogen atom in the N–H···π interaction, while the characteristic peak at 399.69 eV was attributed to the amide nitrogen in MC-LR.[41] In the O 1s spectrum, the characteristic peak at 532.56 eV for C═O in the probe split into two peaks at 531.16 eV and 532.22 eV after interaction, corresponding to the oxygen atom involved in the C–H···O interaction as an electron acceptor and the O–H vibration of the carboxylate group in MC-LR, respectively. The S 2p spectrum showed that the S 2p3/2 peak of the probe's thiophene ring shifted from 164.05 eV to 163.90 eV, with a decrease in the binding energy, indicating an increase in the sulfur atom's electron density, suggesting that the interaction between the probe and the hydrophobic region of MC-LR weakened the conjugation effect of the thiophene ring.[42] Additionally, the increase in the sulfur electron density correlates with the red shift of the thiophene unit's π → π* transition observed in the UV spectra, further supporting the role of long-chain binding in modulating molecular orbital hybridization. XPS analysis reveals that the binding between the probe and MC-LR achieves energy level regulation through directional electron density transfer, optimizing the excited-state decay pathways and ultimately enabling highly sensitive fluorescence responses.

The UV spectra of the probe exhibited significant changes before and after contact with microcystin, indicating alterations in the electronic transition behavior and molecular association states (Fig. 8). In the absence of the toxin (0 μM), the strong absorption band was mainly attributed to π → π* transitions associated with the carbazole moiety and the thiophene unit. The absorbance rapidly decreased beyond 430 nm, suggesting that the probe predominantly exists in a monodispersed state and that electronic transitions within the π-conjugated system are relatively localized. After exposure to the toxin (100 μM), the overall absorbance significantly decreased.[43] This observation indicates that π–π stacking between the probe and the toxin expanded the effective conjugation of the carbazole unit and enhanced excited-state electron delocalization, leading to a red shift of the π → π* transition. Additionally, it is hypothesized that C–H···π, N–H···π, and C–H–O interactions could promote intermolecular charge transfer (ICT), resulting in the appearance of a new absorption peak in the longer wavelength region. The overall decrease in absorbance (0 μM → 100 μM) further reflects the formation of long-chain binding: during the process driven by multiple interactions, some π → π* transitions that were previously allowed may be partially suppressed due to intermolecular orbital overlap; additionally, aggregation-induced light scattering also contributes to the reduced apparent absorbance.[44] Overall, the evolution of the UV spectra is consistent with the electron-density rearrangement revealed by XPS, supporting a

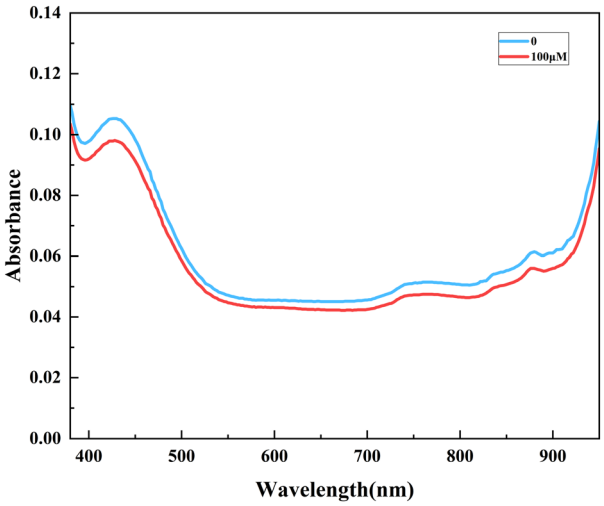

Fig. 8 UV absorption spectra of the probe before and after the reaction.

tendency for electron transfer from the probe to the toxin, which provides the driving force for the fluorescence response.

After contact with microcystin, the fluorescence intensity of the probe increased significantly (approximately twofold at 100 μM compared to 0 μM), accompanied by a red shift of the emission maximum from 606 nm to 610 nm (Fig. 9). This suggests that, in the absence of the toxin (0 μM), the carbazole moiety of the probe retains a certain degree of conformational flexibility, allowing the excited-state energy to be more readily dissipated through nonradiative pathways such as intramolecular vibrations, resulting in weaker fluorescence and a relatively blue-shifted emission. Upon exposure to the toxin, cooperative C–H···π, N–H···π, and C–H···O stacking interactions between the probe and the toxin, along with the binding of the long-chain segment,

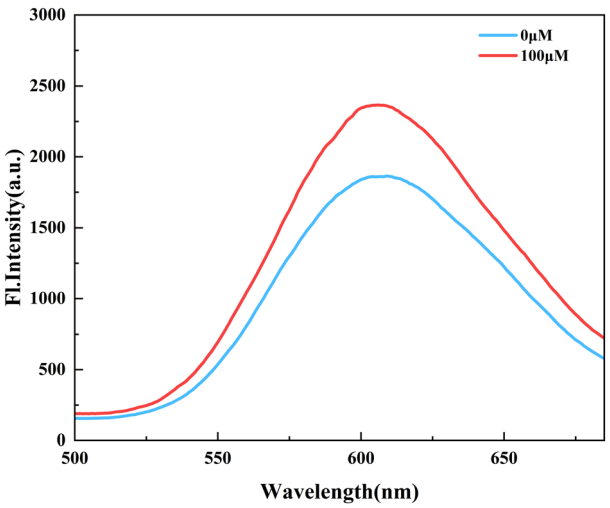

Fig. 9 Fluorescence spectra of the probe before and after the reaction.

enhanced the overall stability of the probe–toxin complex and effectively suppressed nonradiative decay channels, thereby increasing the probability of radiative transitions and leading to fluorescence enhancement. Meanwhile, the improved symmetry of the emission band at 610 nm indicates that intermolecular interactions increased the rigidity of the excited-state structure and reduced the spectral broadening caused by vibrational coupling.[45,46] Combined with the enhanced long-wavelength absorption observed in the UV spectra and the electron density rearrangement revealed by XPS, these phenomena support the presence of multiple noncovalent interactions between the probe and the toxin: π–π stacking and long-chain binding provide the molecular recognition framework, C–H···π, N–H···π, and C–H···O interactions stabilize the complex, and energy-level-matched electron transfer modulates the excited-state decay pathways, ultimately enabling highly sensitive fluorescence detection of MC-LR.

According to Fig. S3–S6, after interaction with MC-LR, both the ^{1}H NMR and ^{13}C NMR spectra of the probe exhibited varying degrees of chemical shift changes, indicating that the local electronic environment surrounding the molecule was significantly altered. The aromatic and conjugated moieties of MC-LR are known to show obvious ^{1}H NMR shift changes after noncovalent inclusion, while the binding-induced redistribution of electron density can also be reflected in the ^{13}C chemical shift changes of adjacent carbon nuclei.[47,48] Therefore, the changes in the ^{1}H NMR and ^{13}C NMR spectra of the probe before and after interaction with MC-LR can be attributed to the combined effects of C–H···π, N–H···π, C–H···O, and hydrophobic long-chain-related interactions, which together induce noncovalent binding and electronic environment rearrangement.[49]

FTIR analysis was performed on the probe before and after interaction with MC-LR to determine whether any new bonding interactions were generated. As shown in Fig. S10, the infrared absorption characteristics of the probe changed markedly after interaction with MC-LR. After reaction, a broader absorption band appeared in the 3600–3000 cm^{-1} region, indicating that the contributions of N–H and O–H related vibrations in the system were significantly enhanced after the introduction of MC-LR. At the same time, a new obvious absorption peak emerged near 1650 cm^{-1}, which was mainly attributed to the C=O stretching vibration of the peptide bond in MC-LR.[50,51] In addition, the peak profile in the 1500–1000 cm^{-1} region also changed significantly compared with that before the reaction, suggesting that the carbonyl groups, aromatic framework, and surrounding chemical environment were rearranged after binding between the probe and MC-LR. The recognition and binding of MC-LR through its aromatic moieties are generally closely associated with π–π interactions and hydrophobic interactions, indicating that its aromatic fragments and hydrophobic chain segments provide a structural basis for noncovalent recognition.[52–54] Therefore, it can be inferred that the probe and MC-LR mainly form a stable complex through the synergistic effects of C–H···π, N–H···π, C–H···O, and hydrophobic long-chain-related interactions. Specifically, the N–H and C–H groups in the amino acid residues of MC-LR may interact with the aromatic rings of the probe through N–H···π and C–H···π interactions, while the polarized C–H groups may also participate in C–H···O interactions. These weak interactions can induce changes in the local electronic environment, which are further reflected in the shifts and variations of the FTIR peaks.[55–57] These results are consistent with the other characterization data and further support the proposed sensing mechanism of the probe.

4. Conclusions

In summary, a small-molecule fluorescent probe was successfully developed for the specific detection of microcystin-LR (MC-LR). The probe exhibited excellent sensitivity toward MC-LR, showing a good linear fluorescence response over the concentration range of 0–100 μM, with a detection limit of 0.507 μM. The fluorescence signal of the probe remained stable over a relatively wide pH range (6–9) and showed excellent photostability. In addition, the probe maintained high selectivity toward MC-LR in the presence of various amino acids, indicating its potential applicability in complex environmental samples. Zebrafish embryo assays further confirmed the low toxicity of the probe, demonstrating its good environmental compatibility. Mechanistic investigations revealed that the fluorescence enhancement was driven by the synergistic effect of multiple noncovalent interactions, including π–π stacking, C–H···O, N–H···π, and C–H···π interactions, together with a long-chain binding effect; these interactions jointly stabilized the probe–toxin complex and facilitated electron transfer. Considering that cyanobacterial blooms usually occur in summer, real environmental water sample experiments were not conducted in this study; such experiments will be further carried out in future work in combination with actual bloom events. These results demonstrate the promising potential of this probe for the rapid and reliable detection of MC-LR in natural water bodies.

Author contributions

Jinfeng Chen: data curation, investigation, writing – review & editing. Zhicen Qiu: data curation, formal analysis, visualization, and writing – original draft. Linyu Fan: data curation and visualization. Yisang Lu: data curation and visualization. Silong Li: data curation and visualization. Yuxin Yang: data curation and visualization. Wanhe Wang: data curation and visualization. Cheuk-Lam Ho: conceptualization, data curation, funding acquisition, investigation, writing – review & editing. Xiao Yao: conceptualization, data curation, funding acquisition, investigation, writing – review & editing. Zhuwu Jiang: conceptualization, data curation, funding acquisition, investigation, writing – review & editing.

Conflicts of interest

The authors declare no conflict of interest.

Data availability

The data that support the findings of this study are available in the supplementary information (SI) of this article.

Supplementary information is available. See DOI: https://doi.org/10.1039/d6sd00036c.

Acknowledgements

This work was supported by the Natural Science Foundation of Fujian Province (2024J08211), the Fujian University of Technology (M82032500335 and KY351616), and the financial support of the Fujian Provincial Department of Finance (GY-Z23273).

References

1 L. Feng, Y. Wang, X. Hou, B. Qin, T. Kutser, F. Qu, N. Chen, H. W. Paerl and C. Zheng, *Nat. Rev. Earth Environ.*, 2024, **5**, 631–644.
2 B. Li, Z. Wang, H. Chuan, J. Li, P. Xie and Y. Liu, *Anal. Chim. Acta*, 2024, **1288**, 342188.
3 C. Liang and X. Ping, *Mini-Rev. Med. Chem.*, 2016, **16**, 1018–1031.
4 J. Qian, L. Qian, N. Pu, Y. Bi, A. Wilhelms and S. Norra, *Environ. Sci. Technol.*, 2024, **58**, 15607–15618.
5 T. Kim, J. Shin, D. Lee, Y. Kim, E. Na, J.-h. Park, C. Lim and Y. Cha, *Water Res.*, 2022, **215**, 118289.
6 S. Merel, D. Walker, R. Chicana, S. Snyder, E. Baurès and O. Thomas, *Environ. Int.*, 2013, **59**, 303–327.
7 S. Zhang, X. Du, H. Liu, M. D. Losiewic, X. Chen, Y. Ma, R. Wang, Z. Tian, L. Shi, H. Guo and H. Zhang, *Environ. Res.*, 2021, **192**, 110254.
8 N. Wei, C. Hu, E. Dittmann, L. Song and N. Gan, *Water Res.*, 2024, **262**, 122119.
9 K. A. Ger, E. J. Faassen, M. G. Pennino and M. Lürling, *Harmful Algae*, 2016, **52**, 34–45.
10 H. k. Kordasht, S. Hassanpour, B. Baradaran, R. Nosrati, M. Hashemzaei, A. Mokhtarzadeh and M. d. la Guardia, *Biosens. Bioelectron.*, 2020, **165**, 112403.
11 H. Zhang, B. Li, Y. Liu, H. Chuan, Y. Liu and P. Xie, *J. Hazard. Mater.*, 2022, **424**, 127406.
12 X. Hu, Z. Wang, X. Ye, P. Xie and Y. Liu, *Environ. Pollut.*, 2024, **342**, 123123.
13 B. Li, Y. Liu, H. Zhang, Y. Liu, Y. Liu and P. Xie, *Coord. Chem. Rev.*, 2021, **443**, 214041.
14 J. A. Cotruvo, *J. AWWA*, 2020, **112**, 84–86.
15 Y. Liu, B. Li, H. Zhang, Y. Liu and P. Xie, *Coord. Chem. Rev.*, 2022, **457**, 214416.
16 L. Chen, R. Tan, Y. Zhou, L. Zhang, S. Zhang, X. Li, Y. Cong, H. Li, P. Sun, H. Ueda and J. Dong, *Microchem. J.*, 2020, **158**, 105325.
17 E. A. Zvereva, O. D. Hendrickson, A. V. Zherdev and B. B. Dzantiev, *Anal. Methods*, 2020, **12**, 392–400.
18 H. B. Bostan, S. M. Taghdisi, J. L. Bowen, N. Demertzis, R. Rezaee, Y. Panahi, A. M. Tsatsakis and G. Karimi, *Biosens. Bioelectron.*, 2018, **119**, 110–118.
19 L. L. Zhang, R. P. Yu, L. P. Wang, S. F. Wu and Q. J. Song, *Environ. Sci.: Processes Impacts*, 2016, **18**, 493–499.
20 S. Adjei-Nimoh, L.-N. Rances, M. A. Tony, H. A. Nabwey and W. H. Lee, *Sci. Rep.*, 2024, **14**, 31968.
21 M. Lee, S. H. Kim, D. Kim and H. J. Kim, *Journal*, 2024, **14**, 37.
22 R. P. Rastogi, R. P. Sinha and A. Incharoensakdi, *Rev. Environ. Sci. Bio/Technol.*, 2014, **13**, 215–249.
23 Y. Zhang, J. K. Whalen, C. Cai, K. Shan and H. Zhou, *Water Res.*, 2023, **233**, 119807.
24 T. Suo, M. Sohail, S. Xie, B. Li, Y. Chen, L. Zhang and X. Zhang, *J. Hazard. Mater.*, 2021, **403**, 123418.
25 M. Zhang, Q. Zhang and L. Ye, *Anal. Bioanal. Chem.*, 2024, **416**, 7131–7140.
26 Y. Liu, B. Li, H. Zhang, Y. Liu and P. Xie, *J. Fluoresc.*, 2022, **32**, 505–519.
27 H. Dai, J. Liu, S. Wang, B. Wang, T. Kai, P. Wu and P. Ding, *Analyst*, 2025, **150**, 1470–1489.
28 W. Xiao, J. Du, Y. Zheng, S. Chen, Z. Liu, F. Chen, F. Liu, B. Li, X. Liu and C. Zhang, *J. Nanobiotechnol.*, 2025, **23**, 67.
29 H. Chuan, B. Li, Z. Wang, J. Li, P. Xie and Y. Liu, *Anal. Chem.*, 2023, **95**, 14219–14227.
30 L. Díez-Quijada, A. I. Prieto, R. Guzmán-Guillén, A. Jos and A. M. Cameán, *Food Chem. Toxicol.*, 2019, **125**, 106–132.
31 X. Jiang, R. Yang, X. Lei, S. Xue, Z. Wang, J. Zhang, L. Yan, Z. Xu, Z. Chen, P. Zou and G. Wang, *J. Fluoresc.*, 2024, **34**, 965–975.
32 Y. Fu and N. S. Finney, *RSC Adv.*, 2018, **8**, 29051–29061.
33 Z. Wang, B. Li, P. Xie and Y. Liu, *Dyes Pigm.*, 2022, **207**, 110672.
34 A. P. M. Antonyraj, P. Nainangu, A. S. Ganeshraja, A. Guru, K. Subramanian, M. D. Tanwar, V. Parimelazhagan and A. S. K. Kumar, *Talanta Open*, 2025, **12**, 100495.
35 R. Payà-Pou, J. Aguirre-Camacho, E. F. Simó-Alfonso, D. Knopp, M. Miró and E. J. Carrasco-Correa, *Microchim. Acta*, 2024, **191**, 490.
36 B. M. Saalidong, S. A. Aram, S. Otu and P. O. Lartey, *PLoS One*, 2022, **17**, e0262117.
37 B. Li, Y. Liu, Y. Liu and P. Xie, *Water Res.*, 2022, **221**, 118811.
38 P. Michaelis, N. Klüver, S. Aulhorn, H. Bohring, J. Bumberger, K. Haase, T. Kuhnert, E. Küster, J. Krüger, T. Luckenbach, R. Massei, L. Nerlich, S. Petruschke, T. Schnicke, A. Schnurpel, S. Scholz, N. Schweiger, D. Sielaff and W. Busch, *Environ. Sci. Technol.*, 2025, **59**, 4304–4317.
39 K. Xu, W. Ai, Q. Wang, L. Tian, D. Liu, Z. Zhuang and J. Wang, *Gondwana Res.*, 2022, **108**, 127–132.
40 G. Stewart, E. M. Alvarez, C. Rapala, J. H. Sklar, J. A. Kalow and C. A. Malapit, *Nat. Synth.*, 2026, **5**, 55–63.
41 N. Wu, W. He, S. Shi, X. Yuan, J. Li, J. Cao, C. Yuan and X. Liu, *J. Colloid Interface Sci.*, 2025, **684**, 658–667.
42 Y. Gui, Y. Wang, D. Wang, Y. Qin, G. Song, D. Yan, B. Z. Tang and D. Wang, *Angew. Chem., Int. Ed.*, 2024, **63**, e202318609.

43 H. Zhang, J. Chen and P. Xie, *Int. J. Biol. Macromol.*, 2025, **298**, 139873.
44 C. M. A. Alves, S. Naik, P. J. G. Coutinho and M. S. T. Gonçalves, *Tetrahedron Lett.*, 2009, **50**, 4470–4474.
45 R.-L. Lin, R. Li, H. Shi, K. Zhang, D. Meng, W.-Q. Sun, K. Chen and J.-X. Liu, *J. Org. Chem.*, 2020, **85**, 3568–3575.
46 Z. Wang, Y. Hao, J. Shen, B. Li, H. Chuan, P. Xie and Y. Liu, *J. Hazard. Mater.*, 2024, **462**, 132771.
47 L. Chen, D. D. Dionysiou and K. O'Shea, *Environ. Sci. Technol.*, 2011, **45**, 2293–2300.
48 A. L. Ptaszek, S. Kratzwald, F. Sagan, M. Migotti, P. A. Sánchez-Murcia, R. Konrat and G. Platzer, *J. Phys. Chem. B*, 2025, **129**, 4917–4928.
49 G. Platzer, M. Mayer, A. Beier, S. Brüschweiler, J. E. Fuchs, H. Engelhardt, L. Geist, G. Bader, J. Schörghuber, R. Lichtenecker, B. Wolkerstorfer, D. Kessler, D. B. McConnell and R. Konrat, *Angew. Chem., Int. Ed.*, 2020, **59**, 14861–14868.
50 A. Barth, *Biochim. Biophys. Acta*, 2007, **1767**, 1073–1101.
51 J. Waeytens, J. De Meutter, E. Goormaghtigh, A. Dazzi and V. Raussens, *Anal. Chem.*, 2023, **95**, 621–627.
52 M. Nishio, *J. Mol. Struct.*, 2012, **1018**, 2–7.
53 W. Y. Sohn, V. Brenner, E. Gloaguen and M. Mons, *Phys. Chem. Chem. Phys.*, 2016, **18**, 29969–29978.
54 Y. Gu, T. Kar and S. Scheiner, *J. Am. Chem. Soc.*, 1999, **121**, 9411–9422.
55 J. L. Roberts, S. G. Zetterholm, L. Gurtowski, P. U. A. I. Fernando, A. Evans, J. Puhnaty, K. M. Wyss, J. M. Tour, B. Fernando, G. Jenness, A. Thompson and C. Griggs, *J. Hazard. Mater.*, 2023, **458**, 131737.
56 W. El Bouaidi, G. Enaime, M. Loudiki, A. Yaacoubi, M. Douma, A. Ounas and M. Lübken, *Journal*, 2022, **10**, 1235.
57 J.-A. Park, J.-K. Kang, S.-M. Jung, J.-W. Choi, S.-H. Lee, V. Yargeau and S.-B. Kim, *Chemosphere*, 2020, **247**, 125811.